X-ray-diffraction study of the lattice distortions induced by a fractional monolayer: ZnTe embedded in vicinal CdTe(001)

N. Boudet,* J. Eymery,† and N. Magnéa
CEA/Grenoble, Département de Recherche Fondamentale sur la Matière, Condensée/SP2M/PSC, 17 rue des Martyrs, F-38054 Grenoble Cedex 9, France
(Received 11 December 1996)

The distortion gradient of the interplanar distances induced by a ZnTe fractional monolayer embedded in vicinal *B*-type CdTe(001) is analyzed within a kinematical model from the diffuse scattering near the (004) Bragg peak of the substrate (scans along [00*l*]). It is explained how these x-ray measurements allow us to extract the relevant structural parameters of the sample. With this method, only the planes with distortions along the growth direction and without local bending give a significant contribution to the diffuse scattering along [00*l*]. The measured diffuse intensity only comes from a fraction of the sample volume. It is shown that the elasticity theory is very well verified in the monolayer limit by comparing the strains predicted by this theory to *ab initio* pseudopotential calculations. By assuming that this approach is still valid in the submonolayer range, the maximum Zn concentration per plane and the integrated Zn quantity are deduced from the distortion curves. The asymmetric profile of the Zn concentration can be explained by a nucleation of ZnTe islands. This analysis of the diffuse scattering has been proven to be very sensitive to the elastic deformation of the layers due to the large lattice mismatch between CdTe and ZnTe (about 6%), but not to the chemical composition of the cationic planes (Cd or Zn). In a more general way, it can easily be applied to systems having a large chemical contrast. [S0163-1829(97)04123-4]

I. INTRODUCTION

Quantum confinement is one of the greatest successes in recent band-gap engineering technology. Quantum wires and dots of II-VI and III-V compound semiconductors exhibit unique optical and electrical properties,[1,2] but the controlled fabrication of these heterostructures remains a difficult task. The couples of materials must be chosen with precise band-gap characteristics, furthermore the heterostructures have to grow coherently (i.e., without dislocation) and with severe size requirements (mean values and fluctuations). Some processes have been developed to build such quantum-sized objects like nanolithography,[3] spontaneous self-organization, or nucleation at the edges of the terraces.[1,2] The crystal lattice between the wires or dots is inhomogeneously strained, mainly due to internal stresses (i.e., lattice mismatch between the materials) and to elastic strain relaxation. It is well known that strains strongly affect the microscopic and the macroscopic properties of semiconductor heterostructures (for example, the band gap and the emission wavelength). The determination of these strains can be performed by grazing incidence x-ray diffraction. Experimentally, several in-plane and out-of-plane diffraction peaks must be measured to know the complete tensor strain components of the heterostructures. For pseudomorphic growth on a thick substrate crystal, the problem is much simpler because the in-plane lattice constants are accommodated to the lattice parameter of the substrate, and so it is only important to know the deformation profile along the growth direction. This deformation profile can be extracted from the analysis of the diffuse diffraction near the Braff peaks of the structure. In this paper, we will show how the deformation profiles along the growth direction, resulting from the insertion of ZnTe fractional monolayers in a CdTe(001) vicinal sample, can be extracted from this technique. An x-ray source with a high brilliance is needed due to the very small amount of ZnTe embedded in the CdTe matrix and the experiments were performed in the European Synchrotron Radiation Facility (ESRF).

ZnTe induces a large stress field in the matrix because of the large lattice mismatch between CdTe and ZnTe (about 6% for the bulk values). The in-plane lattice parameter relaxation of this high strain during the first stages of the ZnTe growth on CdTe(001) have been studied elsewhere.[4] For a fractional layer buried into CdTe, only a distortion of the interplanar distances relaxes the energy of the system in the elastic regime. From the electronic point of view, the ZnTe thin layers (gap=2.39 eV) embedded in the CdTe matrix (gap=1.60 eV) have been demonstrated to be very interesting for assessment of isoelectronic perturbation effects in $CdTe/Cd_xZn_{1-x}Te$ superlattices.[5] Moreover, the insertion of fractional monolayers leads to an interesting localization phenomena like the quantization of the movement of the center of mass of the exciton.[6]

Section II describes the elaboration of the sample and the experimental setup. The simple kinematical model used to extract the relevant structural parameters (deformations, roughness, etc.) from the (00*l*) diffuse scattering curves will be developed in Sec. III. Section IV describes firstly the fitting procedure, then we comment on the values and the correlations of the parameters obtained from the fit of the diffuse scattering around the (004) Bragg reflection. Section V is devoted to the interpretation of the vertical distortions. The validity of linear elasticity is checked within the monolayer limit: the elastic deformation induced by the insertion of one monolayer of ZnTe in CdTe is compared to *ab initio* calculations within a plane-wave orbital basis. By assuming that

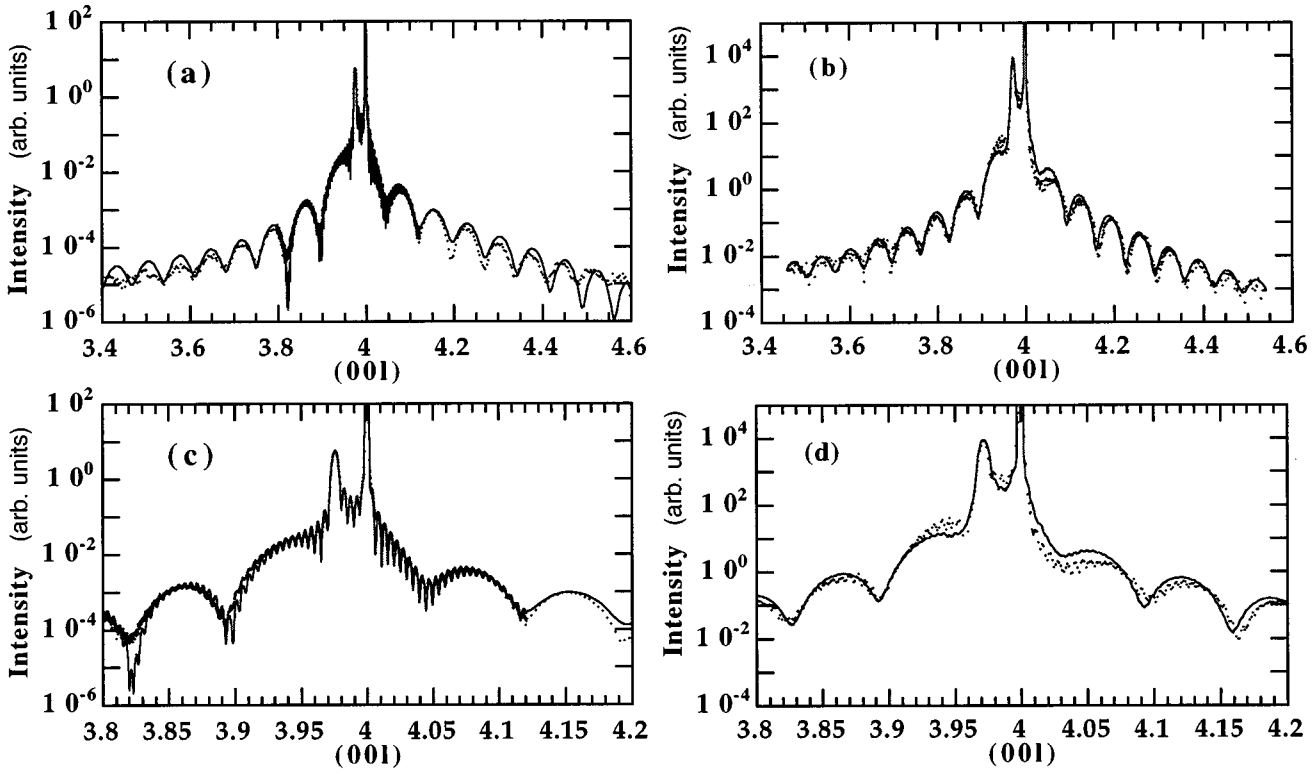

FIG. 1. (a) and (b) Diffuse x-ray scattering intensities of the Z841 and Z952 samples (scan along $[00l]$) near the (004) substrate Bragg peak. l is in reciprocal-lattice unit of the substrate ($2\pi/a_{\mathrm{sub}}$). Dots are measurement data and solid lines correspond to the best fit. (c) and (d) Details of the interference effects presented in (a) and (b) and best fits.

this theory is also valid in the submonolayer limit, it is shown how the deformation profile can be interpreted according to the sample characteristics. It is also shown how the Zn atomic concentration can be estimated from the experimental data. Finally, we summarize our work in Sec. VI.

II. SAMPLES AND EXPERIMENTAL SETUP

The samples under study are grown by conventional molecular beam epitaxy (the detailed conditions for fabrication have been described elsewhere[1]). A CdTe buffer layer (around 1000 Å thick) is grown on a $Cd_{0.96}Zn_{0.04}Te(001)$ substrate with a 2° miscut towards the [110] direction (2° B vicinal surface). A single fraction of ZnTe monolayer is deposited at 320 °C. At this temperature, ZnTe grows at the step edges of the buffer as shown by the disappearance of the oscillation of the reflection high-energy electron specular beam monitoring the deposition. The wires are then encapsulated under approximately 200 Å of CdTe. The samples are kept under vacuum after a short transfer under N_2. Two samples with $\frac{1}{4}$ and $\frac{1}{2}$ ML of ZnTe, named, respectively, Z841 and Z952 in the following, are studied in this paper. The wire thickness is about $a_{\mathrm{ZnTe}}/2 \approx 3$ Å and the average in-plane spacing, about 90 Å, is determined by the miscut of the sample.

X-ray-diffraction experiments were carried out on the CRG-Interface French beam line of the ESRF with the multitechnique goniometer using a radiation wavelength of about 0.6889 Å (18 keV) for sample Z952 and of about 1.2400 Å (10 keV) for sample Z841. The energy was selected with a monochromator made of two Si(111) horizontal crystals, the second one being bent to get a sagittal focusing. Grazing incidence x-ray-diffraction (GIXD) has been performed on the ⟨220⟩ and ⟨440⟩ Bragg reflections to verify the zero in-plane lattice mismatch between the CdTe layer and the substrate: $(\Delta a/a)_{\parallel} = 0.01\%$ for Z952, and this mismatch was too low to be measured with this instrument for Z841. This result confirms the very low density of dislocations in the samples. The miscuts of the samples have been measured by comparing the specular reflected beam and the (004) Bragg reflection. For sample Z841, the miscut is about $2.00° \pm 0.005°$ towards [110] and $0.13° \pm 0.005°$ towards [110]. For sample Z952, these two values are, respectively, $2.10° \pm 0.005°$ and $0.10° \pm 0.005°$. The superlattice peaks due to the periodicity of the Zn growth at the terrace edges (scans along the [110] direction) cannot be clearly measured. Only a diffuse component can be determined indicating a very large fluctuation of the edges.

The diffuse scattering intensity was measured along the $[00l]$ direction around the (004) Bragg peak. This quantity is only sensitive to the crystalline contribution of the sample whose planes are perpendicular to the [001] direction, and it is not sensitive to the in-plane order. The geometry of the experiment consisted in counting scattered photons within the angular acceptance of the detector while symmetrically increasing the incident (α) and exit (β) angles on the $(00l)$ planes by keeping α equal to β. The openings of the slits before and after the sample were set to get a sufficient resolution ($< 6 \times 10^{-3}$ Å^{-1}) to measure the interference fringes due to the largest thickness of the layers of about 1000 Å. The incident beam divergence was $\Delta\theta = 1{,}3$ mrad.

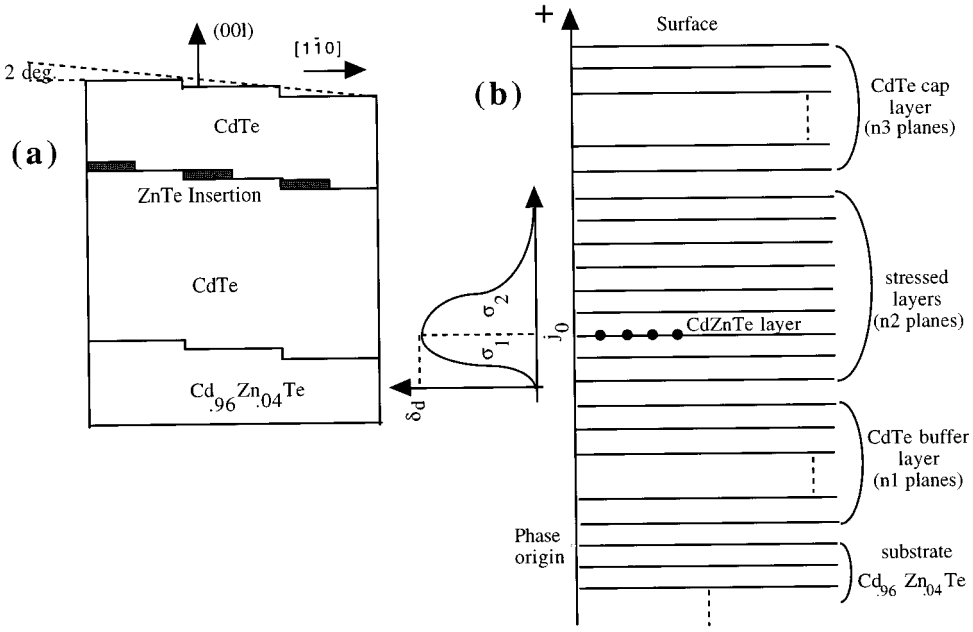

FIG. 2. (a) Schematic representation of the samples studied in this paper (no step meandering is drawn). The diffracting column used in the model is detailed in (b). Along [001], the CdTe structure is formed of pure alternating planes of Cd and Te.

Figure 1 shows a sharp peak at $l=4$ which is the Bragg diffraction peak of the $Cd_{0.96}Zn_{0.04}Te$ substrate. The smaller peak on the left results from the CdTe buffer layer. Two series of interference fringes are shown in this figure resulting from the CdTe buffer and the CdTe cap layer. The fractional insertion of Zn induces a dephasing term between these two contributions. The oscillation periodicity of these fringes in a reciprocal-lattice unit is nearly equal to the inverse of the number of the CdTe unit cells, so that the wider oscillations [see Figs. 1(a) and 1(b)] come from the CdTe cap layer and the thinner [see the zoom in Figs. 1(c) and 1(d)] from the CdTe buffer.

III. CALCULATION MODEL

A. Introduction

We present a simple model based on the kinematical approximation for the treatment of the data shown in Fig. 1. A detailed description of a quite similar method applied to a quantitative analysis of the extended reflectivity curve of a reactional interface SmTe/CdTe is given elsewhere.[7] The sample, shown in Fig. 2(a), is divided into diffracting columns the in-plane extent of which will be discussed later. The structure factor a column is obtained by summing the contribution to the scattered amplitude of different layers [see Fig. 2(b)] which are successively for the sake of simplicity: the substrate, the buffer layer with n_1 alternating planes of Cd and Te, one plane containing x Zn atoms and $1-x$ Cd atoms (x being the fraction of inserted monolayer), and the cap layer (n_3 planes). In fact, the strain of the sample is complex because the ZnTe step decoration introduces a lattice bending of the diffracting planes the in-plane confinement of which depends of the amplitude of the step edges fluctuations. A coherent CdTe column as well as bended planes give no contribution to the diffuse scattering intensity measured only with an out-of-plane momentum transfer. The method presented in this paper is therefore very selective, because only the planes with distortions along the growth direction and without local bending give a significant contribution to the diffuse scattering along $[00l]$. Consequently, the column giving the measured diffuse intensity corresponds to a fraction of the volume bounded by two step edges. Moreover, the x-ray contrast is mainly due to the interplanar distance variation because the influence of the difference between the Cd and Zn form factor ($f_{Cd}=48e^-$ and $f_{Zn}=30e^-$) is smaller than that induced by the large mismatch effect between ZnTe and CdTe.

The substrate and the CdTe lattice parameters along the growth axis, a_{sub} and a_{CdTe}, were precisely measured by high-resolution x-ray diffraction. The interplanar distances $d_{sub}=a_{sub}/4$ and $d_{CdTe}=a_{CdTe}/4$ are, respectively, equal to $d_{sub}=1.616$ Å and $d_{CdTe}=1.626$ Å for sample Z841 and $d_{sub}=1.615$ Å and $d_{CdTe}=1.627$ Å for sample Z952. The interplanar distance under and above the plane containing the Zn fractional layer is written d_{CdTe}-δd.

A very simple model (with only the adjustable parameter δd) consisting in a rectangular shape of the distortion profile is not able to fit correctly the data. The variation δd does not allow us to reproduce properly the change of phase between the amplitudes scattered by the n_1 and n_3 planes, particularly the position of the wider oscillations are not well reproduced. The best fit is however obtained for $\delta d=0.28$ Å in the sample Z841 and $\delta d=0.09$ Å in Z952. It is noteworthy that the value for Z841 is unphysical because the maximum deformation, calculated within the elasticity theory in Sec. V, for a pure ZnTe layer is 0.21 Å.

We tried to improve this simple model by introducing two kinds of perturbation to the perfect structure: firstly, a lateral fluctuation[8] of the parameter δd where the amplitudes and/or the intensities of the diffraction columns are summed with a Gaussian variation. But, the effect of the lateral fluctuations is only to lower the intensity of the wider oscillations, and does not allow us to improve the fit. The second type of defect consists in adding a gradient of interplanar distance along the growth axis near the Zn plane insertion [see Fig. 2(b)]. This latter improves considerably the fit and is fully described in the next section.

TABLE I. Adjusted parameters of the model described in the text. n_1, n_2, n_3 are the number of planes (see Fig. 2), $\sigma_1, \sigma_2, \delta d$ define the deformations of the layer containing ZnTe insertion, β is the roughness parameter, and $\sqrt{\langle z^2 \rangle}$ in the rms roughness. The error bars are only indicative and correspond to a variation of 1% of the χ^2.

Sample	n_1	σ_1	σ_2	n_2	δd (Å)	n_3	β	$\sqrt{\langle z^2 \rangle}$ (Å)
Z841	814±4	0.7±0.5	4.2±0.3	22±3	−0.1±0.005	44±3	0.12±0.1	0.6±0.4
Z952	824±15	0.4±0.3	3.0±0.6	16±3	−0.04±0.01	53±1	0.7±0.1	4.5±3

B. Description of the model

A stressed layer, containing n_2 planes, is introduced between the buffer layer (n_1 planes) and the cap layer (n_3 planes). In the kinematical approximation, the amplitude scattered by one column, $A(q_z)$, is given by

$$A(q_z) = A_{\text{sub}}(q_z) + A_1(q_z) e^{iq_z d_{\text{CdTe}}} + [A_2(q_z) + A_3(q_z) e^{iq_z (d_{\text{CdTe}} + \text{thick2})}] e^{iq_z n_1 d_{\text{CdTe}}}, \tag{1}$$

where A_{sub} is the amplitude scattered by the substrate and A_j the amplitude scattered by the jth layer. Thick2 is the total thickness of the n_2 planes containing the ZnTe fractional insertion. Note that the phase origin is chosen at the top of the substrate [see Fig. 2(b)], this plane is supposed to be Te terminated because of the Te-flux saturation before the beginning of the buffer growth.

The amplitude of the substrate is approximated by

$$A_{\text{sub}}(q_z) = \frac{(f_{\text{Te}} + f_{\text{Cd}} e^{-iq_z d_{\text{sub}}})}{1 - e^{-iq_z 2 d_{\text{sub}}} e^{-v}}, \tag{2}$$

where v takes roughly into account the absorption of the layers: $v \cong 8\pi d_{\text{sub}} / q_z \lambda \Lambda$, where λ is the wavelength and Λ is a characteristic length adjusted to obtain the intensity of the substrate Bragg peak. $f_i(q_z)$ is the form factor of the element i (to simplify the notation, the q_z dependence is omitted in the formulas).

The buffer layer contains n_1 pure Cd and Te planes alternating along [001]. The first plane is a Cd one and two cases have to be taken into account according to the parity of n_1:

$$A_1(q_z) = \begin{cases} \dfrac{(f_{\text{Cd}} + f_{\text{Te}} e^{iq_z d_{\text{CdTe}}})(1 - e^{iq_z (n_1/2) d_{\text{CdTe}}})}{1 - e^{iq_z 2 d_{\text{CdTe}}} e^{-v}} & \text{if } n_1 \text{ is even} \\ \dfrac{(f_{\text{Cd}} + f_{\text{Te}} e^{iq_z d_{\text{CdTe}}})(1 - e^{iq_z [(n_1 - 1)/2] d_{\text{CdTe}}})}{1 - e^{iq_z 2 d_{\text{CdTe}}} e^{-v}} + f_{\text{Cd}} e^{iq_z (n_1 - 1) d_{\text{CdTe}}} & \text{if } n_1 \text{ is odd.} \end{cases} \tag{3}$$

The CdTe-ZnTe-CdTe interface is modeled by adding a gradient of lattice parameter along the growth direction. n_2 planes are supposed to be deformed by the Zn insertion. As shown in Fig. 2(b), the deformation gradient below (above) the Zn plane is modeled by a Gaussian profile defined by its full width at half maximum σ_1 (σ_2). σ_1 and σ_2 are related to n_2 by n_2 = integer part $[4 \times (\sigma_1 + \sigma_2)] + 3$. n_2 is supposed to be odd to simplify the calculation. The distance between the planes $j-1$ and j is then defined by

$$z(j) - z(j-1) = d_{\text{CdTe}} - \delta d \times \exp\left(- \frac{(j - j_0)^2}{2\sigma_i^2} \right). \tag{4}$$

d_{CdTe}-δd is the interplanar distance between the plane j_0 (the position of the Zn fractional layer) and the plane $j_0 + 1$, where $j_0 = (n_2 + 1)/2$.

The amplitude is then

$$A_2(q_z) = \sum_{j=1}^{n_2} f_j e^{iq_z z(j)}. \tag{5}$$

The nature of the $j = 2n+1$ plane depends on the parity of n_1. It follows that if n_1 is even then $f_{2n+1} = f_{\text{Cd}}$ and $f_{2n+2} = f_{\text{Te}}$ and if n_1 is odd then $f_{2n+1} = f_{\text{Te}}$ and $f_{2n+2} = f_{\text{Cd}}$. For the mixed plane containing the Zn fractional insertion, the atomic form factor value is averaged over Zn and Cd atoms according to the x value. But as discussed before, we measure a distortion contrast which is not influenced by the chemical nature of the cations (Zn or Cd).

Finally, the sample is encapsulated under n_3 planes of CdTe. The nature of the first plane still depends on the parity of n_1: if n_1 is even then $f_1 = f_{\text{Te}}$ $f_2 = f_{\text{Cd}}$ and if n_1 is odd then $f_1 = f_{\text{Cd}}$ and $f_2 = f_{\text{Te}}$; it also depends on the parity of n_3:

$$A_3(q_z) = \begin{cases} \dfrac{(f_1 + f_2 e^{iq_z d_{\text{CdTe}}})(1 - e^{iq_z (n_3/2) d_{\text{CdTe}}})}{1 - e^{iq_z 2 d_{\text{CdTe}}} e^{-v}} & \text{if } n_3 \text{ is even} \\ \dfrac{(f_1 + f_2 e^{iq_z d_{\text{CdTe}}})(1 - e^{iq_z [(n_3 - 1)/2] d_{\text{CdTe}}})}{1 - e^{iq_z 2 d_{\text{CdTe}}} e^{-v}} + f_{\text{Cd}} e^{iq_z (n_{3-1}) d_{\text{CdTe}}} & \text{if } n_3 \text{ is odd.} \end{cases} \tag{6}$$

The substrate roughness (parameter β) is supposed to propagate at the upper interfaces. In this model, the diffracting volume is divided in columns and each column has a probability[4,7] $\beta^n \times (1-\beta)$ to have n planes above the last complete plane of the sample. The total intensity is then obtained by multiplying the intensity of each diffracting column by $(1-\beta)^2/[1-2\beta\cos(\pi 1)+\beta^2]$. Within this approximation, the overall root-mean-square (rms) roughness is given by $\sqrt{\langle z^2\rangle}=\sqrt{\beta}/(1-\beta)\times d_{\mathrm{CdTe}}$. Further standard corrections are applied to compare measured and calculated intensities:[9] the Lorentz factor, the polarization factor, the size of the irradiated area, the Debye-Waller factor, and the experimental resolution.

IV. FITTING PROCEDURE AND EXPERIMENTAL RESULTS

The parameters of the model n_1, σ_2, δ_d, n_3, β and a scale factor are adjusted to minimize the merit function:

$$\chi^2=\frac{1}{M-v}\sum_{j=1}^{M}\{I_{\mathrm{calc}(j)}-I_{\mathrm{expt}}(j)\}^2/\sigma^2_{\mathrm{expt}}(j), \qquad (7)$$

where $v=7$ is the number of parameters and M the number of points of the experimental curve ($M=1995$ for Z841 and $M=685$ for Z952). $I_{\mathrm{calc}}(j)$ [$I_{\mathrm{expt}}(j)$] is the calculated [experimental] intensity and $\sigma_{\mathrm{expt}}(j)$ is the standard [statistical] deviation of the measurement at point j. The calculated curve for the best fit is superimposed to the experimental data in Fig. 1.

Since the parameters n_1 and n_3 do not play a major role for the interferences, they are adjusted with a conjugate gradient method so as to calculate the same width of oscillations as the measured one, corresponding, respectively, to the buffer layer and the cap layer (see their values in Table I). During the fitting procedure, the parity of n_1 and n_3 is tested and the diffracted intensity is calculated according to Eqs. (3) and (6). Then, the refinement of the strained layer parameters, σ_1, σ_2, and δd, consists in reproducing the change of phase between the amplitudes scattered by the n_1 and n_3 planes. The calculation of the Hessian matrix of the merit function gives the correlation factors between the parameters of this model. It shows that these three parameters are correlated and their adjustment must be done step by step, after studying their effect on the calculated curve. The measure of the intensity on a wide range of momentum transfer allows us to diminish this correlation: the final values are given in Table I. The error bars on the parameters given in this table are estimated for a 1% variation of the χ^2. The error bars on the correlated parameters are probably underestimated by this method.

δd is smaller than the value found with no gradient (see Sec. III A), but the strain extends on several planes. Moreover, the value of δd is smaller for sample Z952 than for sample Z841: this shows that a smaller quantity of ZnTe was deposited in the first sample. For both samples the gradient is asymmetric (see Fig. 6): it extends on one monolayer (two planes) under the plane containing the Zn insertion and up to 4 ML above it.

β does not play a crucial role on the determination of the gradients of distortion. The experimental curve of sample Z841 is reproduced with a very small interface roughness, $\sqrt{\langle z^2\rangle}<1$ Å, whereas the Z952 one is greater: $\sqrt{\langle z^2\rangle}\approx 4.5$ Å. These values are quite small and show that the roughness of the substrates were small. The value for Z952 has been confirmed by small-angle x-ray reflectivity. With the standard optical transfer-matrix method, the reflectivity curve (not presented in this paper) is fitted with a rms roughness of 4 Å for the substrate, in good agreement with the values determined from large-angle scattering. Unfortunately, small-angle x-ray reflectivity has not been performed on sample Z841. The difference between these two values may be attributed to the sensitivity of the x-ray measurement to the substrate surface preparation.

Note that both experimental curves are well reproduced by calculating the contribution of only one column. For a coherent scattering between N columns, the total scattered amplitude should be

$$F(q_z)=\sum_{j=1}^{N}A(q)e^{iq_z(j-1)d}=A(q)\frac{1-e^{iq_zNd}}{1-e^{iq_zd}}, \qquad (8)$$

where $A(q)$ is the amplitude scattered by one column calculated in Sec. III B and d is the step height. The second term of this equation induces a very strong damping of the intensity which does not correspond to the slow decrease of intensity measured around the (004) Bragg peak. Therefore, it proves that the diffracting columns of this sample are not coherent. This behavior can be explained by the large roughness of the step edges confirmed by grazing incidence x-ray-diffraction measurements. As a matter of fact, Fig. 2(a) is only schematic, and perhaps misleading because the large fluctuations of the terrace length (and also the bending of the planes) are not drawn.

The coherence has been proved[10] to be larger in AlAs/GaAs superlattices grown on a vicinal GaAs substrate, and with a diffracting column consisting in four steps, this indicates the better crystalline quality of these III-V samples. The best fit obtained for the sample Z841 was used to calculate the diffracted intensity around the (002) and (006) Bragg peaks: the experimental and calculated curves are shown in Figs. 3(a) and 3(b). The calculated curves fit well the experimental ones. These two complementary measurements were only performed very close to the Bragg peaks of CdTe and of the substrate, it allows us to verify the consistency of the model, in particular the lattice parameters, the n_1 value, and the interferences close to the Bragg peaks.

The asymmetry of the gradient of the lattice parameter has also been observed for thin ZnTe (and MnTe) epitaxial layers on nominal surfaces. Indeed, the lattice distortion has been directly studied from high-resolution electron microscopy (HREM) images.[11] The samples were observed in a $\langle 110\rangle$ direction, and the local displacements of the (002) planes were measured directly from HREM images (the point to point resolution of the 400-keV microscope was about 1.7 Å. It has been shown that the distortion profiles were asymmetric for 1-,2-,3-ML depositions with residual distortions extending to a few planes on either side of the inserted layers. Furthermore, the maximum measured distortion was less than expected by elastic calculations. It has been interpreted by the presence of nonabrupt interfaces resulting from the interfacial roughness and also from some

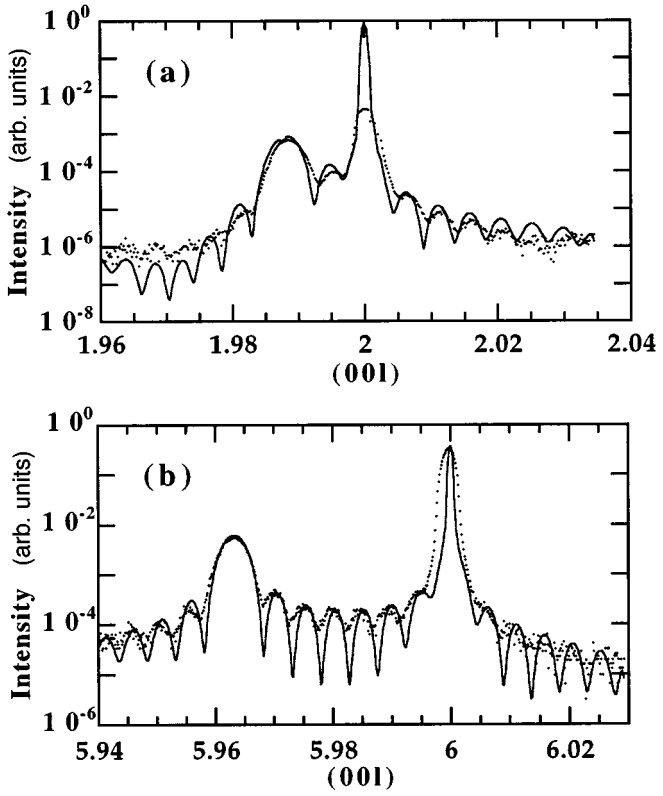

FIG. 3. X-ray-diffraction profiles of the Z841 sample, (a) near the (002) and (b) near the (006) substrate Bragg peaks. The experimental conditions (incident-beam divergence and slits openings) were the same as for the measure around the (004) substrate Bragg peak. The solid curve is calculated with the parameters fitted from the (004) experimental curve (see Fig. 1).

segregation during the growth. This technique has some limitations which do not exist in the diffraction method presented in this paper. (i) The spots correspond to either columns of atom pairs (Cd+Te or Zn+Te), or channels between these atom pairs, so that individual planes are not resolved. (ii) A partial relaxation of the inner strain may occur during the specimen thinning. (iii) The resolution limit is about one monolayer on a nominal surface, and the fractional monolayer deposition on vicinal surfaces is very difficult to study due to the projection effect. Nevertheless, the images represent an average scattering potential through thickness which also integrates nonlinearity of the terrace edges (and of the ZnTe decoration). In the x-ray study presented in this paper, the asymmetry of the gradient is confirmed although the measured signal comes only from the nonbended distorted planes.

V. INTERPRETATION OF VERTICAL LATTICE DISTORTIONS

A. Validity of the linear elasticity within the monolayer limit

The perpendicular strain of a perfect ZnTe monolayer (within a biaxial stress) buried on a CdTe(001) matrix can be calculated from the standard macroscopic elasticity theory by

$$\varepsilon_{\perp}^{\max}=\frac{a_{\mathrm{ZnTe}}^{\perp}-a_{\mathrm{ZnTe}}}{a_{\mathrm{ZnTe}}}=-2\frac{C_{12}^{\mathrm{ZnTe}}}{C_{11}^{\mathrm{ZnTe}}}(a_{\mathrm{CdTe}}-a_{\mathrm{ZnTe}})/a_{\mathrm{ZnTe}}. \tag{9}$$

TABLE II. Comparison between the calculated (plane-wave orbital basis) and the experimental (Refs. 18 and 19) lattice parameter a (Å) and cubic elastic constants C_{11} and C_{12} of CdTe and ZnTe (GPa). For the cubic symmetry, the bulk modulus is related to the elastic constants by $B=(C_{11}+2C_{12})/3$.

Source	a (Å)	C_{11} (GPa)	C_{12} (GPa)	B (GPa)
		CdTe		
Experiments	6.481	53.8	37.5	44.5
This work	6.370	60.5	37.6	45.2
		ZnTe		
Experiments	6.089	71.3	40.7	50.9
This work	5.924	80.8	40.6	54.0

The experimental lattice constants C_{ij}^{ZnTe} and the equilibrium lattice parameters a_k (given in Table II) show that this strain is about -7.53%. This equation can also be written with respect to the substrate bulk lattice parameter as

$$\Delta_{\perp}^{\max}=\frac{a_{\mathrm{ZnTe}}^{\perp}-a_{\mathrm{CdTe}}}{a_{\mathrm{CdTe}}}=\frac{a_{\mathrm{ZnTe}}}{a_{\mathrm{CdTe}}}(1+\varepsilon_{\perp}^{\max})-1$$
$$=-\varepsilon_0\left(1+2\frac{C_{12}^{\mathrm{ZnTe}}}{C_{11}^{\mathrm{ZnTe}}}\right), \tag{10}$$

where $\varepsilon_0=(a_{\mathrm{CdTe}}-a_{\mathrm{ZnTe}})/a_{\mathrm{CdTe}}$.

The numerical value of $\Delta_{\perp}^{\max}$ predicted from this theory is about -12.95%. It can be directly measured from the diffraction experiments. The question is to know if the assumptions of macroscopic elasticity theory can be applied to a monolayer (and later a submonolayer) thin film. High–resolution electron microscopy studies[12] have purported the existence of a severe elastic anomaly for a (001) monolayer of InAs, embedded in GaAs. This system is very close to ZnTe/CdTe(001) with a large misfit of the bulk lattice parameter of about 7% (instead of 6%) and with similar elastic constants. But later, x-ray standing-waves experiments[13] and an *ab initio* calculation[14] have proved that the strains distortions can be accurately described by macroscopic-elastic theory. In our system, we will also prove by *ab initio* calculations that this theory can be applied in the monolayer limit. The problem will be later to extend this assumption to the submonolayer range to estimate the Zn atomic concentration from the lattice distortions.

Total-energy calculations are carried out using the *ab initio* pseudopotential method. Our calculations are performed in the framework of the density-functional theory within the local-density approximation by using the Biosym Program.[15] The soft norm-conserving pseudopotentials of Troullier and Martins,[16] including relativistic corrections, are employed. The program uses nonlinear core corrections to enhance the transferability of the potential. The total energy of the system includes the plane waves with kinetic energy up to ecut=44 Ry corresponding to an average number of plane-waves size below an ecut of about 17 000. This cutoff energy, which depends on the types of atoms in the simulation cell, has been tested to be sufficient for convergence of the total energy. We do not consider 3*d* electrons explicitly for Zn at-

oms, and treat them as the core. The k-point integration was performed on a single point to decrease the computation time of the large cells. The CdTe and ZnTe lattice parameters a_0 are calculated by minimizing the energy E of the primitive cell (with two atoms) according to the volume $V_0 = a_0^3/4$. As shown in Table II, the values are smaller than experiment by 1.7% and 2.7%. The bulk modulus B is defined by $B=(2/9V_0)(\partial^2 E/\partial\varepsilon^2)|_{\varepsilon=0}$, where $\varepsilon=(a-a_0)/a_0$, with a_0 the equilibrium lattice parameter. The deformation ε is always lower than 1.5% in order to get a small variation of the atomic volume and to remain in the linear regime. The calculated values of the bulk modulus are larger than experiment by 1.6% for CdTe and 6.1% for ZnTe. The C_{11} constant is obtained by multiplying the x axis of the cubic cell by $1+\varepsilon$, but keeping the y and z axis the same.[17] The change in strain energy as the function of ε is then $\Delta E/V_0=\frac{1}{2}C_{11}\varepsilon^2+O(\varepsilon^3)$, and the C_{11} constant is simply obtained by fitting the curve $\Delta E/V_0(\varepsilon)$. Finally, the C_{12} constant is extracted from the bulk modulus which is related to the C_{11} and C_{12} elastic constants by $B=(C_{11}+2C_{12})/3$ for a cubic symmetry. The calculated constants given in Table II show a good quantitative agreement with experimental data[18,19] and with other all-electron self-consistent calculations published in the literature.[20–22] The perpendicular strain $\varepsilon_\perp$ estimated with the calculated volume parameters and the elastic constants of the *ab initio* method is -7.56%. This value is in very good agreement with the value of -7.35% computed from the experimental data.

The insertion of ZnTe in a CdTe matrix is simulated by substituting a Cd plane by a Zn plane in the [001] stacking. The simulation cell is a superlattice (with periodic boundary conditions) made of eight planes of Te, seven planes of Cd, and one plane of Zn. The forces are evaluated numerically by means of the Hellmann-Feynman theorem, they are the gradients of the total energy with respect of ion positions. The energy of the crystal is minimized according to the forces applied on each ion. Due to the symmetry of the simulation cell (PMM2, label 25 of the international tables of crystallography), only 16 atoms have to be considered. They are free to relax in the simulation box whose (001) in-plane stress is fixed by the calculated value of the bulk CdTe. The out-of-plane dimension of the box is chosen in order to obtain, after relaxation, the bulk calculated value of the Cd-Te interplanar distance for the planes far from the Zn insertion. The atomic relaxation is stopped when the root mean square of the forces is smaller than 2.5 meV/ Å ($\approx 4\times10^{-12}$ N).

The calculated interplanar distortions are shown in Fig. 4. The profile is symmetric as imposed by the symmetry of the problem, and there is no gradient. Only the interface planes are affected by the Zn insertion with a maximum distortion of about -13.1%, which can be compared to the value of $\Delta_\perp^{\max}=-12.95\%$ determined from the elastic theory. The agreement between the macroscopic elastic theory and the pseudopotential *ab initio* calculation is therefore very good.

All the previous results tend to prove that the continuum elasticity theory can be applied to the monolayer limit in the ZnTe/CdTe system. This assumption will be extended to the submonolayer range.

B. Determination of the Zn atomic concentration from the deformation profiles

If the elasticity theory is assumed to be valid for the ZnTe wires buried into CdTe, the local amount of Zn can be quantified. Two extreme configurations corresponding to different morphologies of the interface of the diffracting column will be considered as model systems: firstly, a homogeneous $Cd_xZn_{1-x}Te$ alloy and secondly, a broad two-dimensional CdTe and ZnTe islands distribution. In the first case, the plane containing the Zn insertion is supposed to be a $Cd_xZn_{1-x}Te$ alloy whose elastic coefficients and lattice parameter are obtained by linear interpolation between those of pure CdTe and ZnTe: $\langle a\rangle = x a_{\mathrm{ZnTe}} + (1-x)a_{\mathrm{CdTe}}$ and $\langle C_{ij}\rangle = x C_{ij}^{\mathrm{ZnTe}} + (1-x)C_{ij}^{\mathrm{CdTe}}$, where x is the fractional coverage resulting from the Zn deposition.

The strain measured according to CdTe is then

$$\Delta_{\mathrm{alloy}} = \frac{\langle a\rangle}{a_{\mathrm{CdTe}}}\left(1-2\frac{\langle C_{12}\rangle}{\langle C_{11}\rangle}(a_{\mathrm{CdTe}}-\langle a\rangle)/\langle a\rangle\right)-1. \quad (11)$$

We get the following second-order equation as a function of x:

$$x^2\varepsilon_0(B^{\mathrm{ZnTe}}-B^{\mathrm{CdTe}}) + x(\varepsilon_0 B^{\mathrm{CdTe}} - \Delta C_{11}\Delta_{\mathrm{alloy}}/3) + C_{11}^{\mathrm{CdTe}}\Delta_{\mathrm{alloy}}/3 = 0, \quad (12)$$

where

$$\varepsilon_0=\frac{a_{\mathrm{CdTe}}-a_{\mathrm{ZnTe}}}{a_{\mathrm{CdTe}}}, \quad B^j=(C_{11}^j+2C_{12}^j)/3,$$

$$\Delta C_{11}=C_{11}^{\mathrm{CdTe}}-C_{12}^{\mathrm{ZnTe}}.$$

The physical solution for x is the positive root of this equation:

$$x=[(\Delta C_{11}\Delta_{\mathrm{alloy}}/3-\varepsilon_0 B^{\mathrm{CdTe}}) - \sqrt{(\varepsilon_0 B^{\mathrm{CdTe}}-\Delta C_{11}\Delta_{\mathrm{alloy}}/3)^2 - \tfrac{4}{3}C_{11}^{\mathrm{CdTe}}\Delta_{\mathrm{alloy}}\varepsilon_0(B^{\mathrm{ZnTe}}-B^{\mathrm{CdTe}})}]/[2\varepsilon_0(B^{\mathrm{ZnTe}}-B^{\mathrm{CdTe}})]. \quad (13)$$

In the second case, we suppose that the CdTe and ZnTe islands are immiscible and keep their elastic constants. The calculated distortions are then averaged afterward (CdTe islands do not contribute to the crystal deformation in this approach). In this model, x is simply given by

$$x=\Delta/\Delta_\perp^{\max}. \quad (14)$$

This second approximation is not very realistic, but allows us to estimate the error bars occurring when a simple elastic theory is used to extract the chemical composition from the measured distortions. It is important to note that the two approaches fulfill the boundary conditions: $\lim_{\Delta_{\mathrm{alloy}}\to 0} x = 0$ and $\lim_{\Delta_{\mathrm{alloy}}\to\Delta_\parallel^{\max}} x = 1$.

As show in Fig. 5, the discrepancy between these two models is very small (inferior to 2.6% for the whole composition range). Consequently, the function $x(\Delta)=\Delta/\Delta_{\perp}^{\max}$ will be chosen to extract the atomic Zn concentration from the distortion curves (note that this approximation overestimates the Zn concentration).

It is quite difficult to go beyond these two approximation. Finite element or path-integral methods[23] have to be used to take into account the real boundary conditions of a wire embedded in a material. Furthermore, all the fluctuations and average effects have to be introduced if we want to compare the calculations to the experiments. For a perfect linear wire deposited on a substrate surface, the elasticity theory can be much more developed and takes into account the different substrate orientations and the directions of the wires.[24]

The Zn concentrations are integrated on the whole range of the gradients shown in Fig. 6 according to Eq. (14).[25] We find an equivalent amount of ZnTe of 1.5 ML for sample Z841 and 0.5 ML for Z952, which is in agreement with the simple rectangular-shape model values of about 1.3 and 0.46, respectively. The maxima of the distortion curves in Fig. 6 give an estimation of the maximum Zn concentration per plane: 46% and 21% instead of 50% and 25% for the nominal depositions. So, the Zn concentration is slightly underestimated by the analysis of x-ray data compared to the nominal deposition estimated from the growth flux, but the discrepancy is small and probably under the error bars of the experiment and of its modelization. The value of the integrated Zn amount is larger than the nominal deposition because the diffracting column takes into account only a fraction of the sample volume. The very large meandering of the wires and the substrate roughness can also modify the result of the integration and explain the presence of a gradient. The asymmetric profile of Zn concentration has already been observed in thicker samples.[11] It has been attributed to the influence of the growth conditions: the Zn segregation, the beginning of 3D nucleation at the step edges or the interface roughness. In our case, the probability to nucleate ZnTe islands also increases with the ZnTe surface coverage, and

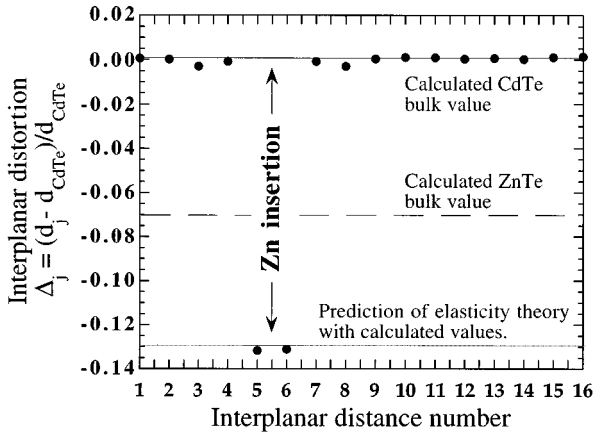

FIG. 4. Lattice distortions of a periodic superlattice made of eight planes of Te, seven planes of Cd, and one plane of Zn (the insertion layer) calculated with the pseudopotential local-density approximation method and compared to the elasticity theory predictions. The deformation is measured with respect to the CdTe host material.

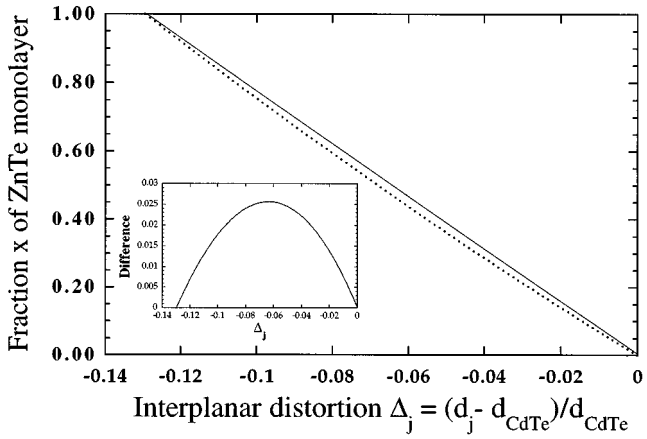

FIG. 5. Curves giving the fraction of ZnTe monolayer for two models. (a) The plane of insertion is supposed to be an alloy (dotted curve): Vegard's law is used for the lattice parameters and an arithmetic mean for the elastic constants is performed. (b) CdTe and ZnTe islands are supposed to be immiscible and keep their elastic constants (full line). The inset shows the absolute value of the difference between these two models. The numerical values used to draw these curves are given in Table II [experimental parameters (Ref. 25)].

similarly explanations can be given. Other techniques, like scanning tunneling microscopy, will be useful to clarify this point.

VI. CONCLUSIONS

It has been shown that the gradients of the interplanar distances resulting from the insertion of a single fractional ZnTe monolayer into a *B* vicinal CdTe substrate can be determined from the analysis of the diffuse scattering near the Bragg peaks of the substrate. It is explained how these x-ray measurements allow us to extract the relevant structural parameters of the sample, in particular the number of planes (in the buffer layer and the cap layer) and the deformations. We have shown that this method is very sensitive to the elastic deformation of the layers, but not to the chemical composi-

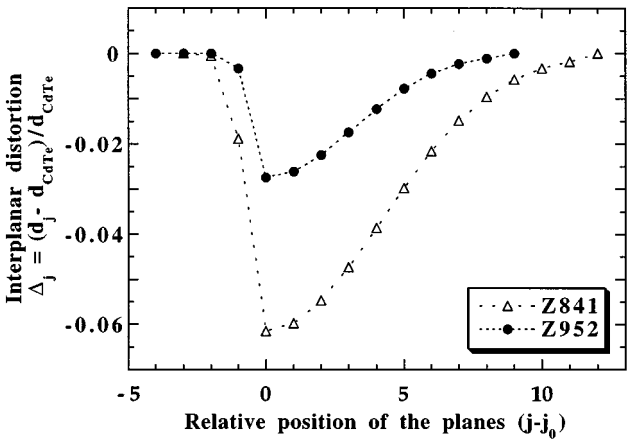

FIG. 6. Gradient of interplanar distances with respect to CdTe deduced from the fit of the diffraction data (see Fig. 1) for the Z841 and Z952 samples.

tion of the cationic planes (Cd or Zn). A gradient of the interplanar distances along the growth axis near the Zn plane insertion must be introduced to treat the data. The asymmetric shape of the distortion profile, already observed in high-resolution microscopy[11] for samples with 1, 2, and 3 ZnTe ML has been confirmed.

It has been checked that the elasticity theory is very well verified in the monolayer limit by comparing the strains predicted by this theory to *ab initio* pseudopotential calculations. By assuming that this approach is still valid in the submonolayer range, the compositions can be estimated from the strain-composition function knowledge. The maxima of the distortion curves give an estimation of the maximum Zn concentration per plane which agrees with the nominal depositions. The value of the integrated Zn amount is found to be larger than the nominal deposition because this x-ray technique is only sensitive to a fraction of the sample. The very large meandering of the wires and the substrate roughness can also modify the result of the integration. The asymmetric profile of Zn concentration can be explained by a nucleation of ZnTe islands as reported in thicker samples.[11] The method presented in this paper has been applied to heterostructures presenting a large mismatch of the lattice parameter. In the CdTe/ZnTe system, the chemical contrast does not play a key role in the interpretation of intensity measurements. For other systems, the chemical contrast can be easily taken into account with nearly the same formalism.

ACKNOWLEDGMENTS

We would like to thank F. Rieutord, R. Simon, and M. Alba for their assistance in x-ray measurements and A. Bourret for stimulating discussions. We are particularly grateful to the staff of the BM32 Interface French Collaborating Research Group of the ESRF (European Radiation Synchrotron Radiation Facility).

*Present address: CEA/Grenoble, Département de Recherche Fondamentale sur la Matière Consensée/SI3M, 17 rue des Martyrs, F-38054 Grenable Cedex 9, France. Electronic address: nboudet@cea.Fr

†Electronic address: jeymery@cea.Fr

[1] N. Magnéa, J. Cryst. Growth **138**, 550 (1994).

[2] J. M. Moison, F. Houzay, F. Barthe, L. Leprince, E. André, and O. Vatel, Appl. Phys. Lett. **64**, 196 (1994).

[3] L. Tapfer, G. C. La Rocca, H. Lage, O. Brandt, D. Heitmann, and K. Ploog, Appl. Surf. Sci. **60**, 517 (1992).

[4] J. Eymery, B. Daudin, S. Tatarenko, D. Brun-Le Cunff, and N. Boudet, Appl. Phys. Lett. **66**, 3456 (1995); J. Eymery, S. Tatarenko, N. Bouchet, and K. Saminadayer, *ibid.* **64**, 3631 (1994).

[5] N. T. Pelekanos, P. Peyla, Le Si Dang, P. H. Jouneau, A. Tardot, and N. Magnéa, Phys. Rev. B **48**, 1517 (1993).

[6] Q. X. Zhao, N. Magnéa, and J. L. Pautrat, Phys. Rev. B **52**, 16 612 (1995).

[7] N. Boudet, J. Eymery, G. Renaud, J. L. Rouvière, J. Y. Veuillen, D. Brun, and B. Daudin, Surf. Sci. **327**, L515 (1995).

[8] P. F. Miceli, C. J. Palmstrøm, and K. W. Moyers, Appl. Phys. Lett. **61**, 2060 (1992).

[9] Doon Gibbs, B. M. Ocko, D. M. Zehner, and S. G. J. Mochrie, Phys. Rev. B **38**, 7303 (1988).

[10] S. K. Sinha, M. K. Sanyal, S. K. Satija, C. F. Majkrzak, D. A. Neumann, H. Homma, S. Szpala, A. Gibaud, and H. Morkoc, Physica B **198**, 72 (1994).

[11] P. H. Jouneau, A. Tardot, G. Feuillet, H. Mariette, and J. Cibert, J. Appl. Phys. **75**, 7310 (1994).

[12] O. Brandt, K. Ploog, R. Bierwolf, and M. Hohenstein, Phys. Rev. Lett. **68**, 1339 (1992).

[13] J. C. Woicik *et al.*, Appl. Phys. Lett. **68**, 3010 (1996).

[14] J. E. Bernard and A. Zunger, Appl. Phys. Lett. **65**, 165 (1994).

[15] *Plane Wave User Guide* (Biosym/Molecular Simulations, San Diego, 1995), Release 3.0.0.

[16] N. Troullier and J. L. Martins, Solid State Commun. **74**, 613 (1990).

[17] J. Eymery, F. Lançon, and L. Billard, J. Phys. (France) I **3**, 787 (1993).

[18] R. D. Greenough and S. B. Palmer, J. Phys. D **6**, 587 (1973).

[19] D. Berlincourt, H. Jaffe, and L. R. Shiozawa, Phys. Rev. **129**, 1009 (1963).

[20] S.-H. Wei and A. Zunger, Phys. Rev. B **37**, 8958 (1988).

[21] A. Continenza and S. Massida, Phys. Rev. B **50**, 11 949 (1994).

[22] G. D. Lee, M. H. Lee, and J. Ihm, Phys. Rev. B **52**, 1459 (1995).

[23] D. A. Faux, J. R. Downes, and E. P. O'Reilly, J. Appl. Phys. **80**, 2515 (1996).

[24] L. De Caro and L. Tapfer, Phys. Rev. B **49**, 11 127 (1994); L. De Caro and L. Tapfer, *ibid.* **51**, 4381 (1995).

[25] Figure 5 is calculated with bulk CdTe lattice parameters $d_{\mathrm{CdTe}} = 1.620$ Å. In the samples, CdTe is strained along the growth axis to $d_{\mathrm{CdTe}} = 1.626$ Å for sample Z841 and to $d_{\mathrm{CdTe}} = 1.627$ Å for sample Z952. These differences do not give significant changes to the curves presented in Fig. 5.